

Fabrication and characterization of cylindrical light diffusers comprised of shape memory polymer

Ward Small IV
Patrick R. Buckley
Thomas S. Wilson
Jeffrey M. Loge
Kristen D. Maitland
Duncan J. Maitland

Lawrence Livermore National Laboratory
7000 East Avenue, L-211
Livermore, California 94550
E-mail: small3@llnl.gov

Abstract. We developed a technique for constructing light diffusing devices comprised of a flexible shape memory polymer (SMP) cylindrical diffuser attached to the tip of an optical fiber. The devices are fabricated by casting an SMP rod over the cleaved tip of an optical fiber and media blasting the SMP rod to create a light diffusing surface. The axial and polar emission profiles and circumferential (azimuthal) uniformity are characterized for various blasting pressures, nozzle-to-sample distances, and nozzle translation speeds. The diffusers are generally strongly forward-directed and consistently withstand over 8 W of incident IR laser light without suffering damage when immersed in water. These devices are suitable for various endoluminal and interstitial biomedical applications. © 2008 Society of Photo-Optical Instrumentation Engineers. [DOI: 10.1117/1.2904952]

Keywords: diffuser; fiber optics; laser; shape memory polymer.

Paper 07051RR received Feb. 14, 2007; revised manuscript received Nov. 27, 2007; accepted for publication Nov. 28, 2007; published online Apr. 30, 2008.

1 Introduction

Cylindrical light diffusing devices are used in various interstitial and endoluminal biomedical applications including thermal laser therapies^{1,2} and photodynamic therapy.^{3–7} Our group has also used them for *in vitro* photothermal actuation of endovascular prototype devices including embolic foams to fill aneurysms^{8,9} and self-expanding stents.¹⁰ The diffuser is generally located at the end of a flexible optical fiber and is guided to the target through a needle, catheter, or endoscope. The required optical and mechanical characteristics of the light-diffusing device are application-dependent. Optical characteristics including the light emission profile and the power-handling capability, together with the tissue absorption and scattering properties, govern the amount and distribution of light delivered to the target tissue volume. Mechanical characteristics including diffuser length, diameter, and flexibility determine where in the body the device can be delivered.

Several techniques have been employed to construct cylindrical light diffusing devices, including etching the end of an optical fiber,^{11–13} adding a diffusing tip comprised of embedded light scattering particles to the end of an optical fiber,^{11,12} and writing a grating into an optical fiber using an excimer laser.¹⁴ Because different diffuser types emit light differently, accurate light dosimetry in the target tissue depends on understanding the light distribution for the particular type of diffuser. Light diffusion measurement systems have been constructed to characterize the axial and circumferential (azimuthal) light emission profiles by sampling discrete points along the diffuser¹⁵ or imaging the entire diffuser.^{12,16} In addition to the axial and circumferential (azimuthal) directions, measurement of the polar radiance distribution has been per-

formed to provide a more thorough assessment of the diffuser emission.^{17–19}

We have developed a technique for constructing high-power light diffusing devices comprised of a flexible shape memory polymer (SMP) cylindrical diffuser attached to the tip of an optical fiber. These diffusers were initially developed to provide a means of photothermal actuation for the devices mentioned previously,^{8–10} though other applications are possible. In addition to possessing shape memory ability [see Figs. 1(a)–1(c)], the stiffness and emission profile of these SMP diffusers can be tailored to suit a particular application, and are therefore novel compared to other commercially available biomedical cylindrical diffusers. Device fabrication procedures are described and the results of optical testing, including axial and polar profiles, circumferential (azimuthal) uniformity, and damage threshold, are presented.

2 Materials and Methods

2.1 SMP

A thermoset SMP formulation developed in-house²⁰ was used to construct the cylindrical diffuser. It was specifically designed to have low absorption in the visible and near-IR spectral regions, as shown in Fig. 2(a) to enable laser light transmission. By modifying the chemical composition of the SMP, the soft phase glass transition temperature (T_g) can be adjusted from 34 to 86 °C, resulting in an elastic modulus from approximately 10⁷ Pa (rubber-like) to 10⁹ Pa (glasslike), respectively, at body temperature²⁰ (37 °C). This feature enables the flexibility of the diffuser to be tailored to the application. In addition, SMP has the unique ability to recover a programmed shape via a thermal actuation mechanism. When sufficiently below its T_g , the SMP can maintain a secondary

Address all correspondence to Ward Small, Lawrence Livermore National Laboratory, L-211-7000 East Avenue, Livermore, CA 94550; Tel: 925-422-1961; Fax: 925-424-2778; E-mail: small3@llnl.gov

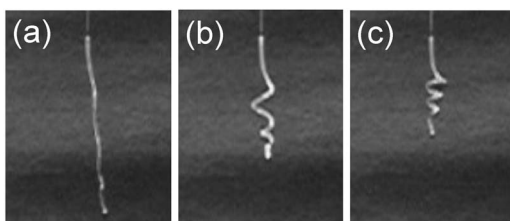


Fig. 1 (a) to (c) Series of images showing a cylindrical SMP rod ($380\ \mu\text{m}$ diameter) attached to a $100\text{-}\mu\text{m}$ -core optical fiber undergoing thermally induced shape recovery from a secondary straight form to its programmed coil form. The SMP was doped with a laser-absorbing dye to enable laser heating. The SMP diffusers could be similarly programmed to change shape if desired. An IR diode laser was used as the actuation source.

shape that is different than its original programmed shape. For the thermoset SMP, the programming occurs during casting (i.e., the cast shape is held in “memory”). The secondary shape is obtained by reforming the SMP while heated slightly above T_g and then cooling to stabilize the new shape. As the temperature is increased to T_g , the SMP will transform back to its programmed shape. Examples of shape recovery by laser heating are illustrated in Figs. 1(a)–1(c).

2.2 Device Fabrication

The light diffusing devices were made by first injection molding the thermoset SMP ($T_g=81^\circ\text{C}$) around the end of a cleaved $100\text{-}\mu\text{m}$ -core silica optical fiber (FIP100110125, Polymicro Technologies, LLC, Phoenix, Arizona) using a Teflon tube with an inner diameter of $1\ \text{mm}$ or $300\ \mu\text{m}$ as the casting mold. The inner diameter of the casting tube was larger than the optical fiber diameter. Therefore, a smaller Teflon tube collar was positioned over the optical fiber (between the optical fiber and the casting tube) to approximately center the optical fiber tip in the casting tube. As the SMP was thermally cured, it bonded with the optical fiber, creating a strong joint without requiring additional adhesives or mechanical fixtures. An image of a joint between an optical fiber ($125\ \mu\text{m}$ diameter) and a cast SMP rod ($300\ \mu\text{m}$ diameter) is shown in Fig. 2(b).

An abrasive media blasting system was built to create a diffusing surface on the SMP rod. The abrasive material ($100\text{-}\mu\text{m}$ sodium bicarbonate particles) was fed through a media blasting machine (MicroBlaster MB1000-1, Comco, Inc., Burbank, California) modified for low-pressure operation ($60\ \text{psi}$ maximum). The blasting nozzle ($800\ \mu\text{m}$ opening) was mounted on a motorized translation stage and the SMP rod sample was fixed on a motorized rotation stage; both stages were controlled using LabVIEW software (National Instruments Corp., Austin, Texas). Beginning near the distal end of the SMP rod, the nozzle was translated $3\ \text{cm}$ along the longitudinal axis of the SMP rod as the SMP rod rotated at $48\ \text{rpm}$ around its longitudinal axis to expose the entire circumference to the abrasive media stream. The blasting pressure ($10, 30, 50\ \text{psi}$), nozzle-to-sample distance ($1, 2, 3\ \text{cm}$), and nozzle translation speed ($1, 2, 3\ \text{mm/s}$) were systematically varied to assess their effects on the emission profile and diffusion efficiency (percentage of incident light emitted outward from the abraded surface of the SMP rod).

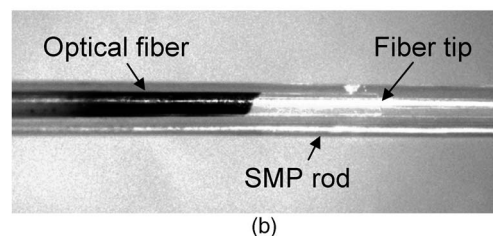
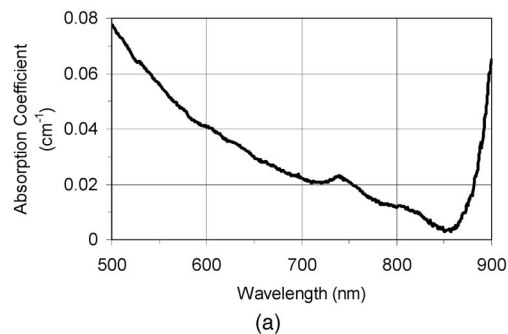


Fig. 2 (a) Absorption coefficient of the SMP as a function of wavelength. Absorbance data was acquired using a Cary 300 spectrophotometer (Varian, Inc., Palo Alto, CA). (b) Microscope image of an SMP diffuser showing the optical fiber ($125\ \mu\text{m}$ diameter including the polyimide coating) embedded in an SMP rod ($300\ \mu\text{m}$ diameter). The polyimide coating was burned off of the optical fiber prior to cleaving the tip.

2.3 Optical Characterization

A 4-mW , 670-nm diode laser module (Coherent Inc., Auburn, California) was used to characterize the diffuser output, which is wavelength-dependent. For the systematic parameter study, 1-mm -diam SMP rods were cast without optical fibers to accelerate the fabrication process. For these samples, the proximal end of the diffuser was faced using a stainless steel blade in a guillotine-style fixture to provide a flat end surface. The laser light was coupled into the diffuser using a fiber collimation lens (F220SMA-B, Thorlabs, Inc., Newton, New Jersey). The lens focused the laser beam onto the proximal end of the SMP rod; the first $4\ \text{cm}$ of the 8.5-cm -long SMP rod was not abraded as this area was concealed by the fixture used to hold the SMP rod in place, and the last $1.5\ \text{cm}$ was also not abraded.

The theoretical half-angle of the cone of light launched in the SMP rod for the lens and fiber coupling schemes was calculated using Snell's law and the following actual values: SMP refractive index = 1.58 , lens diameter = $6\ \text{mm}$, lens focal length = $11\ \text{mm}$, diode laser elliptical beam major axis = $4\ \text{mm}$ and minor axis = $1\ \text{mm}$, fiber core refractive index = 1.4571 , fiber numerical aperture = 0.22 in air. For the fiber-coupled diffuser, the theoretical half-angle emitted by the optical fiber embedded in the SMP rod is 8.0° . For the lens-coupled diffuser, the theoretical half-angles corresponding to the major and minor axes of the laser beam are 6.5° and 1.6° , respectively. Ignoring scattering at the abraded surface, the theoretical numerical aperture (NA) of the SMP rod in air is 1.22 and the critical angle for total internal reflection (θ_c) is 51° (with respect to the rod axis).

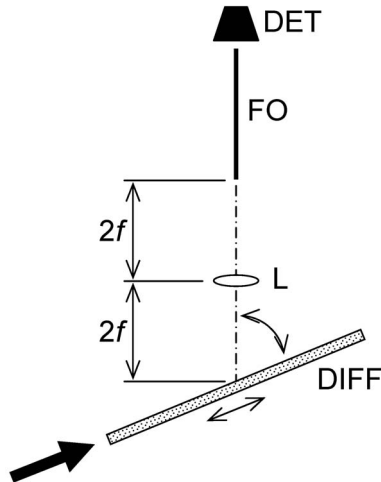


Fig. 3 Schematic diagram of the goniometric apparatus used to characterize the polar light distribution. The SMP diffuser is mounted on a translation/rotation stage, enabling measurement at various axial locations along the diffuser length and polar angles from -65 deg (backward emission) up to 70 deg (forward emission). A polar angle of 0 deg corresponds to perpendicular emission. Laser light is coupled into the diffuser in the direction indicated by the large arrow. DIFF, SMP diffuser; L, imaging lens with focal length f ; FO, $600\text{-}\mu\text{m}$ -core fiber optic; DET, detector.

To measure the axial light emission profile along the length of the diffuser, a 12-bit gray-scale image of the emitting diffuser was acquired using a CCD camera (CoolSNAP HQ, Photometrics, Tucson, Arizona) fitted with a Fujinon 1:1.7/35-mm lens and 5-mm extension tube. The diffuser was manually rotated and reimaged to assess the circumferential (azimuthal) uniformity. MATLAB (The MathWorks, Inc., Natick, Massachusetts) software was used to calculate the average pixel intensity across the width of the diffuser, which was plotted as a function of axial distance along the diffuser length. After each 12-bit image was read into a matrix, the diffuser was segmented using the Sobel method of edge detection provided in MATLAB. The segmented objects were eroded and dilated using a 5×5 -pixel square structuring element to remove background objects. The average pixel intensity value for each axial section of the diffuser was calculated by summing the pixel values in a section and averaging over the diffuser width. The magnification of the imaging system resulted in sections $36.5\ \mu\text{m}$ thick. To ascertain trends in the data, the $36.5\text{-}\mu\text{m}$ section values were passed through a five-point average moving filter, effectively analyzing $146\text{-}\mu\text{m}$ sections without reducing the number of data points.

Based on the system described by Murrer et al.,¹⁷ a goniometric apparatus (Fig. 3) was built to characterize the polar light distribution for a given axial position. The diffuser was mounted on a combination translation/rotation stage. A lens (F220SMA-B, Thorlabs, Inc., Newton, New Jersey) with a focal length of $11.0\ \text{mm}$ was used to image (1:1) an element of the diffuser onto the cleaved face of a $600\text{-}\mu\text{m}$ -core optical fiber. The other end of the optical fiber was directed to a power meter (LABMASTER-E power meter with LM-2 detector head and preamplifier, Coherent Inc.) shielded from ambient light.

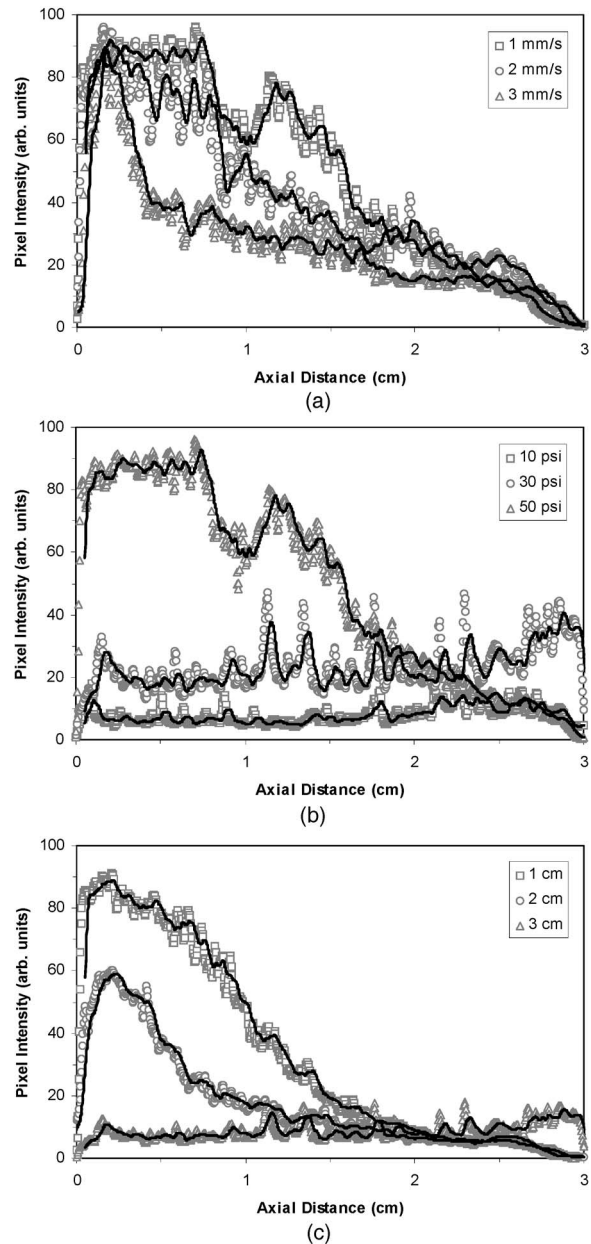


Fig. 4 Selected axial emission profiles illustrating the effect of changing the (a) nozzle translation speed, (b) blasting pressure, and (c) nozzle-to-sample distance for the 1-mm-diam diffusers. In (a), the nozzle-to-sample distance was $3\ \text{cm}$ and the blasting pressure was $50\ \text{psi}$. In (b), the nozzle-to-sample distance was $3\ \text{cm}$ and the nozzle translation speed was $1\ \text{mm/s}$. In (c), the nozzle translation speed was $1\ \text{mm/s}$ and the blasting pressure was $30\ \text{psi}$. The curves were normalized based on the amount of light emitted over the entire 3-cm length, measured using the integrating sphere system.

An integrating sphere (70491, Oriel Instruments, Stratford, Connecticut) with a photodiode (PIN-10DF, UDT Sensors, Inc., Hawthorne, California) was used to measure the diffusion efficiency. The photodiode current, which was amplified using a current amplifier (13AMP005, Melles Griot, Irvine, California), varied linearly with the radiant power. First, the total radiant power emitted from the diffuser, including light emitted from the diffusing surface and from the distal end,

Table 1 Diffusion efficiencies (%) of the 1-mm-diam, 3-cm-long diffusers over axial distances of 1, 2, and 3 cm (values separated by commas)^a for various nozzle-to-sample distances ($D=1, 2,$ and 3 cm), nozzle translation speeds ($S=1, 2,$ and 3 mm/s), and blasting pressures ($P=10, 30,$ and 50 psi).

	$D=1$ cm	$D=2$ cm	$D=3$ cm
$S=1$ mm/s			
$P=10$ psi	39, 71, 91 (9)	12, 31, 60 (40)	5, 10, 18 (82)
$P=30$ psi	75, 94, 98 (2)	70, 91, 97 (3)	13, 29, 47 (53)
$P=50$ psi	54, 81, 90 (10)	77, 90, 94 (6)	63, 89, 96 (4)
$S=2$ mm/s			
$P=10$ psi	10, 29, 62 (38)	13, 26, 41 (59)	6, 13, 23 (77)
$P=30$ psi	25, 55, 79 (21)	45, 73, 90 (10)	40, 68, 86 (14)
$P=50$ psi	39, 74, 91 (9)	67, 91, 96 (4)	61, 87, 96 (4)
$S=3$ mm/s			
$P=10$ psi	17, 32, 51 (49)	13, 31, 49 (51)	1, 6, 12 (88)
$P=30$ psi	25, 45, 65 (35)	32, 63, 81 (19)	17, 31, 47 (53)
$P=50$ psi	43, 69, 82 (18)	58, 89, 98 (2)	55, 83, 94 (6)

^aThe first three values represent the percentage of incident light emitted over the first 1 cm of diffuser length, the first 2 cm of diffuser length, and the entire 3 cm, respectively. The fourth value (in parentheses) represents the percentage of incident light exiting the distal end of the diffuser and is equal to the difference between the diffusion efficiency over 3 cm and 100%. For example, a perfectly uniform diffuser with a diffusion efficiency of 90% over 3 cm would have values of 30, 60, and 90% with 10% exiting the distal end.

was measured by inserting the entire diffuser through an aperture slightly larger than the diffuser diameter into the integrating sphere. The diffuser was then withdrawn in 1-cm increments and the power emitted from the distal portion inside the sphere was measured. The difference between the total power and each distal power was then divided by the total power to obtain the diffusion efficiency (percentage of incident light emitted outward) over lengths of 1, 2, and 3 cm.

Since the optical characterization instrumentation was designed for straight diffusers, a simulation was conducted to compare the emission of straight and curved (270-deg bend) diffusers using ZEMAX ray tracing software (ZEMAX Development Corporation, Bellevue, Washington). The embedded fiber coupling scheme was modeled. The Gaussian scattering model in ZEMAX was employed on the abraded surface to simulate the strongly forward-directed emission observed empirically. Virtual annular detectors (inner diameter=1 mm, outer diameter=5 mm) placed at 1-cm intervals along the length and a virtual circular detector (diameter=1 mm) placed at the distal end of each diffuser recorded the diffuser emission and amount of light exiting the distal end, respectively.

To determine the power-handling capability of the fiber-coupled diffuser in air, an 808-nm fiber-coupled diode laser (UM7800/100/20, Unique-m.o.d.e., Jena, Germany) was connected to the optical fiber. The distal end of a 300- μ m-diam diffuser was inserted into the integrating sphere assembly previously described to monitor the light transmission through the diffuser. The laser power was stepped up in 1-W incre-

ments every 30 s until the photodiode signal suddenly dropped, indicating that the SMP thermal damage threshold had been exceeded. The experiment was conducted for four different diffusers. In addition, diffusers submerged in 37°C (body temperature) water were subjected to laser powers up to 8.6 W and the extent of thermal damage was assessed.

3 Results and Discussion

As shown in Fig. 4, the nozzle translation speed, blasting pressure, and nozzle-to-sample distance can be adjusted to tailor the emission profile from predominantly proximal emission to axially uniform emission. The diffusion efficiencies of the 1-mm-diam diffusers over axial distances of 1, 2, and 3 cm are listed in Table 1 for the various blasting parameters. More severe media blasting (i.e., higher blasting pressure, shorter nozzle-to-sample distance, and/or slower nozzle translation speed) generally resulted in more light emission proximally; less severe media blasting tended to yield more uniform axial emission. There was a trade-off between axial uniformity and the diffusion efficiency over the entire 3-cm length, though diffusers emitting 80 to 90% of the incident laser light fairly uniformly over a length of 3 cm were created. One possible method of increasing the amount of light emitted outward is to incorporate a reflective surface at the distal end of the diffuser. Light that would otherwise exit from the distal end of the SMP rod would be reflected back into the rod and possibly be emitted outward. Future devices may include such a feature.

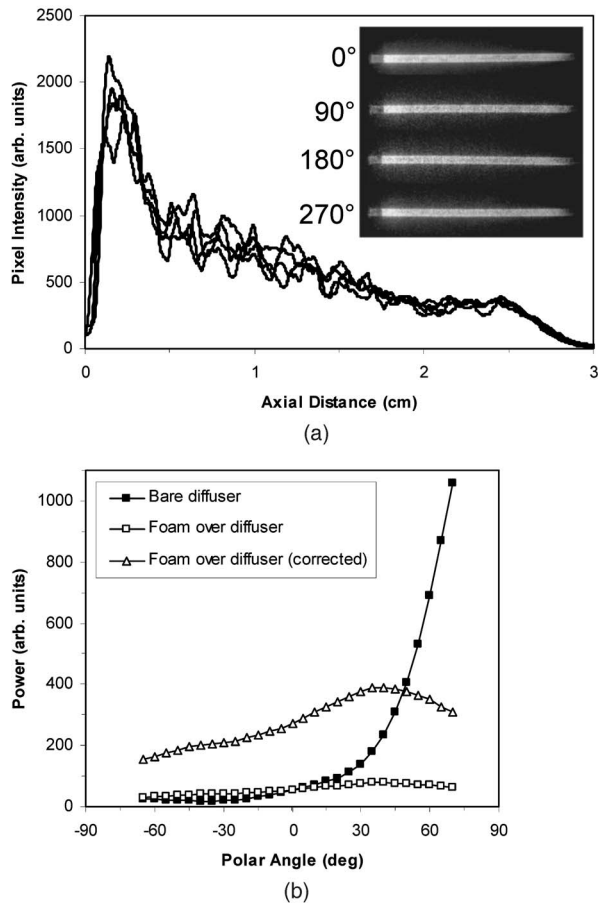


Fig. 5 (a) Axial emission profiles and images of a single 1-mm-diam diffuser acquired at azimuth angles of 0, 90, 180, and 270 deg to illustrate the circumferential uniformity and (b) polar emission profile at an axial distance of 0.5 cm of a 1-mm-diam bare diffuser and the same diffuser surrounded by a 1.5-mm-thick SMP foam collar. In (b), a “corrected” foam-covered diffuser curve is included to better illustrate the redistribution of the emitted light. The curve was obtained by increasing the measured power values by a factor of 5 to approximately compensate for the reduced irradiance at the surface imaged by the goniometer due to the $4\times$ increase in diameter and $\sim 20\%$ loss due to absorption by the foam (measured using the integrating sphere). In (a) and (b), the diffuser was made using a nozzle translation speed of 3 mm/s, a blasting pressure of 50 psi, and a nozzle-to-sample distance of 3 cm.

As shown in Fig. 5(a), the emitted light is circumferentially uniform and strongly forward-directed. The strongly forward-directed emission in air becomes more isotropic in interstitial applications such as photodynamic therapy (PDT) since the tissue further scatters light.¹⁷ This is also the case for photothermally actuated SMP porous foam devices,^{8,9} which inherently scatter light, resulting in more symmetric heating of the SMP foam volume. This was demonstrated by the flattened polar emission profile of a diffuser surrounded by an SMP foam collar shown in Fig. 5(b). In addition to increasing the overall outward emission, the addition of a reflective surface at the distal end may also increase the amount of backward-directed emission, improving the polar uniformity. Appropriate combinations of blasting parameters required for

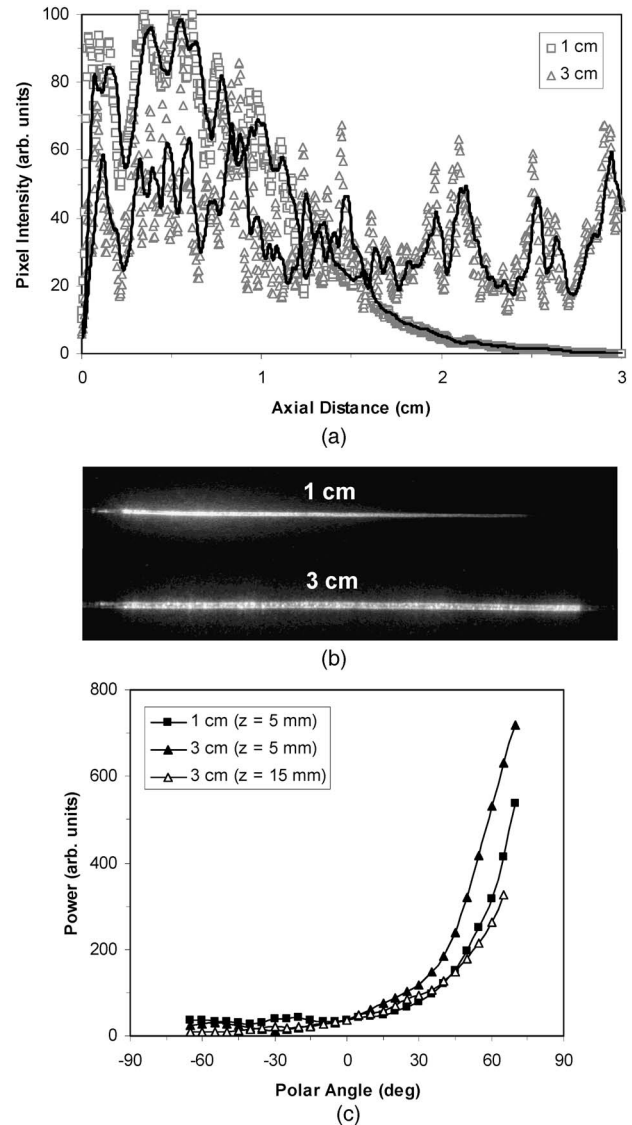


Fig. 6 (a) Axial emission profiles and (b) images of 300- μm -diam diffusers created using nozzle-to-sample distances D of 1 and 3 cm. In (a), the curves were normalized based on the amount of light emitted over the entire 3-cm length measured using the integrating sphere system. The diffusion efficiencies over axial distances of 1, 2, and 3 cm were 82, 99, and 100%, respectively, for $D=1$ cm and 37, 68, and 91%, respectively, for $D=3$ cm. (c) Polar emission profiles of the diffusers in (a) and (b) at axial distances of 0.5 cm ($D=1$ and 3 cm) and 1.5 cm ($D=3$ cm only). In (c), the curves were normalized to have equal power at a polar angle of 0 deg (perpendicular to diffuser axis). In (a) to (c), the nozzle translation speed and blasting pressure were 3 mm/s and 40 psi, respectively.

optimal performance of a reflective-tipped diffuser may be investigated in future work.

Similar to the results for the 1-mm-diam diffusers, we created 300- μm -diam diffusers that radially emit over 80% of the incident light over a length of 1 cm, as shown in Fig. 6(a) and 6(b); these diffusers were designed for use with our embolic foam devices.^{8,9} By increasing the nozzle-to-sample distance, we also created 300- μm -diam diffusers that radially emit 100% of the incident laser light nearly uniformly over a

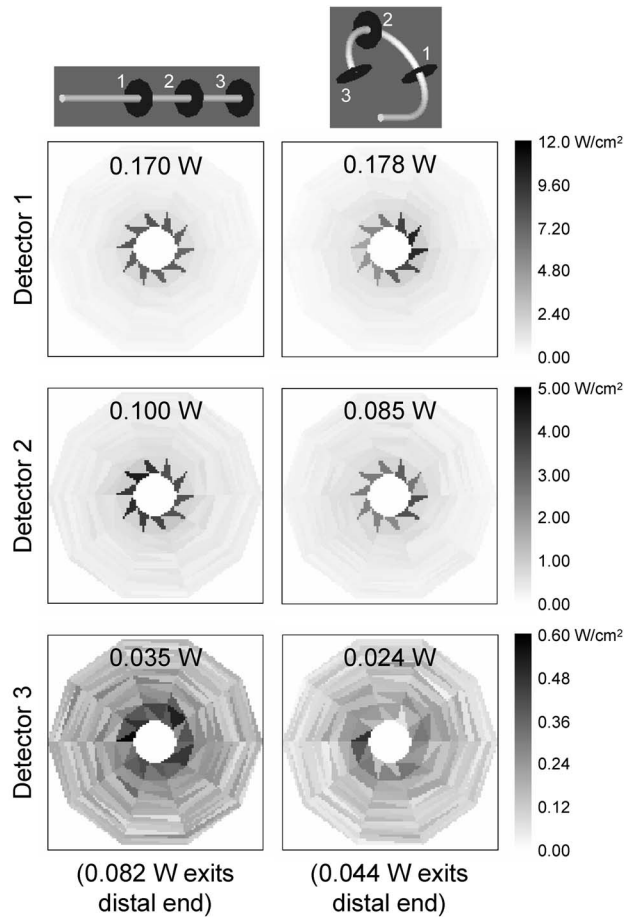


Fig. 7 ZEMAX simulation comparing the emission of straight (left column) and curved (right column) 1-mm-diam, 3-cm-long diffusers. The radius of curvature of the curved diffuser is 6.366 mm and the bend angle is 270 deg. A total power of 1 W was launched from the embedded fiber. The irradiance at the surface of each of the three virtual annular detectors is plotted and the total incident power is noted for each diffuser. The power exiting the distal end of each diffuser is also noted. The detector surfaces are comprised of triangular pixels.

length of 3 cm, which is desirable for *in situ* photoactivation of PDT drugs. Figure 6(c) indicates the forward-directed nature of the emission for the 300- μm diffusers.

Results of the ZEMAX simulation comparing the emission of 1-mm-diam, 3-cm-long straight and curved diffusers are shown in Fig. 7. The virtual detectors collecting the emitted light indicate similar axial, polar, and circumferential (azimuthal) emission for the straight and curved diffusers. Different curved geometries will yield different results.

The distribution of optical transmission modes in the SMP diffusers affects the emission profile. The axial distance required to achieve equilibrium mode distribution (EMD) in a 1-mm-diam plastic step-index optical fiber ($\text{NA}=0.51$, $\theta_c=20$ deg) is approximately^{21,22} 20 m, a length much greater than the SMP diffusers in this study. However, EMD is achieved in a much shorter axial distance for the SMP diffusers as a result of scattering at the abraded surface in addition to diffraction by microscopic defects in the SMP rod such as diameter changes, cracks, voids, and density fluctuations.²² The mode coupling was assessed by observing the far-field

intensity pattern emitted from the distal end of the lens-coupled 1-mm-diam 8.5-cm-long SMP rods (both the proximal and distal ends were polished using lapping paper) with and without diffusing regions. The 3-cm-long diffusing regions were created using blasting pressures of 10 and 50 psi, respectively, at a nozzle translation speed of 3 mm/s and a nozzle-to-sample distance of 3 cm. The far-field intensity pattern emitted from a nondiffusing SMP rod (surface not abraded) was a donut comprising higher order modes indicating EMD was not achieved^{21,22} (higher order modes did not significantly couple into lower order modes). The donut pattern, which can be generated from a multimode fiber-coupled diode laser,²³ indicates that the lower order modes initially launched into the SMP rod were suppressed or redistributed into higher order modes. The far-field intensity pattern for the SMP diffuser created at 10 psi indicated significant coupling of higher order modes into lower order modes. The far-field intensity pattern for the SMP diffuser created at 50 psi was approximately a disk with its peak intensity at the center suggesting nearly complete mode filling.^{21,22} Based on these results, the fiber-coupled 300- μm -diam SMP diffusers in this study are also expected to achieve significant mode filling.

The thermal damage threshold at the laser wavelength of 808 nm [SMP absorption coefficient $\approx 0.01 \text{ cm}^{-1}$, see Fig. 2(a)] for each of four 300- μm -diam diffusers was reached after 10 s at 6 W, 15 s at 8 W, 8 s at 7 W, and 4 s at 3 W, respectively. On visual inspection, the point of failure was observed near the tip of the 100- μm -core optical fiber, where the power density in the SMP rod is at a maximum. The cause of the relatively low threshold of the fourth diffuser is unknown, though it may be related to the absorption of back-directed laser light by the burnt polyimide coating. Investigation of diffusers created using alternative polyimide removal techniques or polished fibers (no polyimide removal) may provide additional insight.

For endovascular or interstitial applications, the diffusers would be surrounded by blood or tissue, not air. When submerged in water (zero flow) during *in vitro* device actuation experiments, diffusers consistently withstood 8.6 W for ~ 1 min without suffering thermal damage. The efficient cooling provided by the surrounding fluid raised the thermal damage threshold of the SMP relative to that in air. For applications that do not require such small diffusers, using a larger core optical fiber would reduce the power density, potentially further increasing the thermal damage threshold and, hence, the maximum output power.

4 Conclusion

We demonstrated fabrication of SMP cylindrical diffusers mounted on optical fibers for use in endoluminal and interstitial biomedical applications. The fabrication process utilized a combination of injection molding to form the SMP cylinder around the optical fiber and media blasting to create the diffusing surface. The T_g of the SMP can be chosen to provide the appropriate degree of flexibility for the application and the media-blasting parameters can be adjusted to yield the desired axial emission profile. In general, the diffusers were strongly forward-directed and withstood up to 8 W of incident infrared laser light without suffering damage.

Acknowledgments

The authors thank Erica Gjersing for her work on the MAT-LAB program. This work was performed under the auspices of the U.S. Department of Energy by Lawrence Livermore National Laboratory in part under Contract W-7405-Eng-48 and in part under Contract DE-AC52-07NA27344 and supported by the National Institutes of Health/National Institute of Biomedical Imaging and Bioengineering Grant R01EB000462 and Lawrence Livermore National Laboratory Directed Research and Development (LDRD) Grants 04-LW-054 and 04-ERD-093.

References

1. F. Izzo, "Other thermal ablation techniques: microwave and interstitial laser ablation of liver tumors," *Ann. Surg. Oncol.* **10**, 491–497 (2003).
2. D. L. Ware, P. Boor, C. Yang, A. Gowda, J. J. Grady, and M. Motamedi, "Slow intramural heating with diffused laser light: a unique method for deep myocardial coagulation," *Circulation* **99**, 1630–1636 (1999).
3. B. F. Overholt, M. Panjehpour, and J. M. Haydek, "Photodynamic therapy for Barrett's esophagus: follow up in 100 patients," *Gastrointest. Endosc.* **49**, 1–7 (1999).
4. M. Pai, W. Jamal, A. Mosse, C. Bishop, S. Bown, and J. McEwan, "Inhibition of in-stent restenosis in rabbit iliac arteries with photodynamic therapy," *Eur. J. Vasc. Endovasc. Surg.* **30**, 573–581 (2005).
5. S. G. Rockson, D. P. Lorenz, W.-F. Cheong, and K. W. Woodburn, "Photoangioplasty: an emerging clinical cardiovascular role for photodynamic therapy," *Circulation* **102**, 591–596 (2000).
6. L. K. Lee, C. Whitehurst, M. L. Pantelides, and J. V. Moore, "An interstitial light assembly for photodynamic therapy in prostatic carcinoma," *BJU Int.* **84**, 821–826 (1999).
7. F. H. van Duijnhoven, J. P. Rovers, K. Engelmann, Z. Krajina, S. F. Purkiss, F. A. N. Zoetmulder, T. J. Vogl, and O. T. Terpstra, "Photodynamic therapy with 5,10,15,20-tetrakis(*m*-hydroxyphenyl) bacteriochlorin for colorectal liver metastases is safe and feasible: results from a phase I study," *Ann. Surg. Oncol.* **12**, 808–816 (2005).
8. W. Small IV, P. R. Buckley, T. S. Wilson, W. J. Bennett, J. Hartman, D. Saloner, and D. J. Maitland, "Shape memory polymer stent with expandable foam: a new concept for endovascular embolization of fusiform aneurysms," *IEEE Trans. Biomed. Eng.* **54**(Part II), 1157–1160 (2007).
9. D. J. Maitland, W. Small IV, J. M. Ortega, P. R. Buckley, J. Rodriguez, J. Hartman, and T. S. Wilson, "Prototype laser-activated shape memory polymer foam device for embolic treatment of aneurysms," *J. Biomed. Opt.* **12**, 030504 (2007).
10. G. M. Baer, W. Small IV, T. S. Wilson, W. J. Bennett, D. L. Matthews, J. Hartman, and D. J. Maitland, "Fabrication and *in vitro* deployment of a laser-activated shape memory polymer vascular stent," *Biomed. Eng. Online* **6**, 43 (2007).
11. A. C. Lytle, H. L. Narciso, D. V. Spain, and D. R. Doiron, "Third generation cylindrical diffusers for medical use," *Proc. SPIE* **1893**, 195–201 (1993).
12. P. M. Ripley, A. J. MacRobert, T. N. Mills, and S. G. Bown, "A comparative optical analysis of cylindrical diffuser fibres for laser therapy using fluorescence imaging," *Lasers Med. Sci.* **14**, 257–268 (1999).
13. C. T. Germer, D. Albrecht, C. Isbert, J. Ritz, A. Roggan, and H. J. Buhr, "Diffusing fibre tip for the minimally invasive treatment of liver tumours by interstitial laser coagulation (ILC): an experimental ex vivo study," *Lasers Med. Sci.* **14**, 32–39 (1999).
14. L. Vesselov, W. Whittington, and L. Lilge, "Design and performance of thin cylindrical diffusers created in Ge-doped multimode optical fibers," *Appl. Opt.* **44**, 2754–2758 (2005).
15. R. L. Kozodoy, S. L. Lundahl, D. Bell, and J. A. Harrington, "Three-dimensional characterization of the light distribution from diffusing cylindrical optical-fiber tips," *Appl. Opt.* **33**, 6674–6682 (1994).
16. P. M. Ripley, T. N. Mills, and J. A. S. Brookes, "Measurement of the emission profiles of cylindrical light diffusers using a video technique," *Lasers Med. Sci.* **14**, 67–72 (1999).
17. L. H. P. Murrer, J. P. A. Marijnissen, and W. M. Star, "Light distribution by linear diffusing sources for photodynamic therapy," *Phys. Med. Biol.* **41**, 951–961 (1996).
18. L. H. P. Murrer, J. P. A. Marijnissen, and W. M. Star, "Improvements in the design of linear diffusers for photodynamic therapy," *Phys. Med. Biol.* **42**, 1461–1464 (1997).
19. L. M. Vesselov, W. Whittington, and L. Lilge, "Performance evaluation of cylindrical fiber optic light diffusers for biomedical applications," *Lasers Surg. Med.* **34**, 348–351 (2004).
20. T. S. Wilson, W. Small IV, W. J. Bennett, J. P. Bearinger, and D. J. Maitland, "Shape memory polymer therapeutic devices for stroke," *Proc. SPIE* **6007**, 157–164 (2005).
21. A. Djordjevich and S. Savovic, "Investigation of mode coupling in step index plastic optical fibers using the power flow equation," *IEEE Photonics Technol. Lett.* **12**, 1489–1491 (2000).
22. G. Jiang, R. F. Shi, and A. F. Garito, "Mode coupling and equilibrium mode distribution conditions in plastic optical fibers," *IEEE Photonics Technol. Lett.* **9**, 1128–1130 (1997).
23. Y. F. Chen, Y. P. Lan, and S. C. Wang, "Generation of Laguerre-Gaussian modes in fiber-coupled laser diode end-pumped lasers," *Appl. Phys. B* **72**, 167–170 (2001).